Transverse mode locking of different frequency-degenerate families based on annular beam pumping

SHUNQIN ZHANG,[1] ZENAN FU,[1] LINQUAN LAI,[1] FUQIANG JIA,[1,*] DUN QIAO,[2] YUANLONG FAN,[2] KANG LI,[2] AND NIGEL COPNER[2]

[1]*School of Electronic Science and Engineering, Xiamen University, Xiamen, 361005, China*
[2]*Faculty of Computing, Engineering & Science, University of South Wales, Wales, CF37 1DL, UK*
**Corresponding author: jiafq@xmu.edu.cn*

Received XX Month XXXX; revised XX Month, XXXX; accepted XX Month XXXX; posted XX Month XXXX (Doc. ID XXXXX); published XX Month XXXX

Optical vortex arrays have been achieved in an end-pumped Nd:YVO_4 laser pumped by an annular beam. Spontaneous transverse mode locking of Laguerre-Gaussian modes in different frequency-degenerate families has been obtained by merely adjusting the pump power. The maximum output power of 0.88 W and the optical conversion efficiency of 13.6% are achieved for optical vortex arrays. Optical vortex arrays formed in different frequency-degenerate families of Laguerre-Gaussian modes can be actively controlled by the position of the axicon. This work provides a way to research transverse mode locking of Laguerre-Gaussian modes in different frequency-degenerate families based on annular beam pumping.

Vortex beams carry orbital angular momentum (OAM) of $l\hbar$ per photon with helical phase front characterized by the factor $\exp(il\theta)$, where l is the topological charge [1]. Compared to the conventional vortex beams with doughnut-shaped intensity profile, optical vortex arrays (OVAs) possess intriguing transverse patterns and multiple phase singularities. Strong requirements of OVAs have been put forward because of the boom of special applications such as Bose–Einstein condensate [2], manipulating multiple micro-particles [3], optical modulation and communication [4] and 3D displays [5]. In addition to external cavity methods using the liquid crystal layer [6,7] or spatial light modulator [8,9], OVAs have been primarily generated by the intra-cavity methods [10-15] basing on the dynamic characteristics of class-B lasers such as carbon dioxide (CO_2) and solid-state lasers. Generally speaking, each transverse mode oscillated in a laser cavity has its own frequency, but for Laguerre-Gaussian (LG) modes, LG_{pl} modes satisfying $2p+|l|=q$ with q fixed have a common frequency, namely, a frequency-degenerate family [16] of LG modes. OVAs formed in a single frequency-degenerate family of LG modes have been well studied in a gas laser [16] and in vertical-cavity surface-emitting lasers (VCSELs) [17] theoretically and experimentally.

However, transverse mode locking (TML) [18] of LG modes in different frequency-degenerate families has received less attention and only a few articles have reported this phenomenon. Compare to longitudinal mode locking, TML is relatively new, but it has been found to be used for forming OVAs recently. Spontaneous generation of orbital angular momentum crystals using a monolithic Nd:YAG nonplanar ring laser were produced by Lin *et al.* [15] but the laser cavity was relatively complicated. Yu *et al.* [19] reported a self-frequency doubling microchip laser to produce OVA patterns with combination of two frequency-degenerate families. However, the observed patterns, which were not very obvious, were slightly different from the theoretical results. Toda *et al.* [20] used sub-picosecond pulses combined with the second-harmonic to produce a paired OVA. High-order transverse modes have also been achieved by a decentered Gaussian beam pumped microchip laser [21]. Subsequently, they have studied a decentered annular beam pumped dual-vortex laser [22], whose orientation and separation between two holes could be controlled precisely. However, the laser cavity was unable to produce more interesting patterns stemmed from superposition of different high-order frequency-degenerate families. Zhang *et al.* [23-25] demonstrated intra-cavity generation of linearly distributed and continuously varied OVAs, and theoretically analyzed TML of LG modes in different frequency-degenerate families. Meanwhile, annular beam pumping [26] has been proved to be an effective way in the end-pumped solid-state laser for directly generating vortices, which has good spatial overlapping with target LG modes in the gain medium. Unfortunately, it was usually used to produce a single LG mode rather than OVAs.

In this paper, we experimentally demonstrate OVAs formation from an annular beam pumped Nd:YVO_4 laser originates from the TML of LG modes. As far as we know, this is the first time to achieve spontaneous TML of different frequency-degenerate transverse modes pumped by an annular beam. OVAs generation of LG modes in different frequency-degenerate families can be actively switched by adjusting the position of the axicon.

LG modes are a set of solutions of the paraxial wave equation derived in cylindrical coordinates in a laser cavity, for which the

electric field can be expressed as [13]:

$$LG_{p,l} = \sqrt{\frac{2p!}{\pi(p+|l|)!}}\frac{1}{w}\left(\frac{\sqrt{2}r}{w}\right)^{|l|}L_p^{|l|}\left(\frac{2r^2}{w^2}\right)\exp\left(-\frac{r^2}{w^2}-ik\frac{r^2}{2R}\right) \times\exp(-il\varphi)\exp\left[-i(2p+|l|+1)\arctan\left(\frac{z}{z_R}\right)\right] \quad (1)$$

where $L_p^l(\cdot)$ is the generalized Laguerre polynomial with radial and azimuthal indices of p and l, r and φ are the radial and azimuthal coordinates, respectively. Z_R is the Rayleigh length, the radius of curvature r and the spot radius w are dependent on Z. To effectively calculate the beam profile, the low Fresnel number condition is applied, so the TML of different frequency-degenerate transverse modes [25] can be written as:

$$u = \sum_{p,l} g_{p,l} LG_{p,l}(\cdot)\exp\left[-i\varphi_{p,l} - ik\frac{r^2}{2\bar{R}} - i\bar{k}\arctan\left(\frac{z}{z_R}\right)\right] \quad (2)$$

Where $g_{p,l}$ is the relative ratio of different modes, $LG_{p,l}(\cdot)$ is the pure intensity items of LG modes, $\varphi_{p,l}$ is the locked phases of LG modes. $\bar{R}$ and $\bar{k}$ are the average radius of curvature and average total index, respectively. From the formula (2), it is obvious that the field formed by the TML of different frequency-degenerate transverse modes shares the common phase items, which should be considered as a single mode once the TML occurs. Therefore, OVAs with temporal and spatial stability can be gained by above-mentioned conditions.

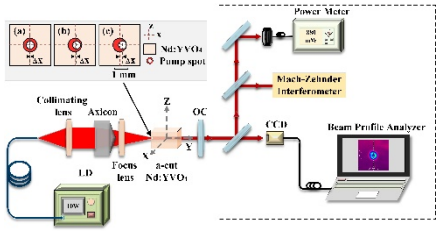

Fig. 1. Schematic of an annular pumped Nd:YVO4 laser for generating vortex array beams, the dotted part represents the subsequent measuring part. Insets depict the incident pump spot on crystal surface for cases (a) Δx=0.00 mm, (b) Δx=0.05 mm, (c) Δx=0.10 mm.

The experimental setup for generating OVAs based on spontaneous TML is shown in Fig. 1. The pump source is an 808 nm fiber-coupled laser diode (LD) with a core diameter of 400 μm and a numerical aperture of 0.22, whose maximum power is 10 W. The pump beam is collimated with a plane-convex lens, then reshaped by an axicon (Thorlabs AX125-B) and a plane-convex lens, as a result, a focused annular pump beam [27] is formed around the focal plane, the focal length of both the lenses is 10 mm. The schematic incident pump spots on crystal surface are shown in the insets of Fig. 1. A three-dimensional coordinate system is introduced into the left surface of the laser crystal and the y-axis is along with the direction of the output laser propagation. The decentered distance Δx can be controlled by adjusting the axicon along the x-axis. When Δx=0.00 mm, the inner and outer diameter are about 0.6 mm and 1.0 mm, as shown in Fig.1(a). And the Fresnel number [10] can be calculated as 5.5, which is beneficial to sustain more multi-transverse modes.

The laser material used in our experiments is a 3 mm ×3 mm ×5 mm a-cut Nd:YVO_4 crystal with 0.5 at.% doping concentration. The crystal is wrapped with indium foil and mounted in the copper heat sink. The temperature of laser crystal is actively controlled at 12℃ by a thermoelectric cooler (TEC) which is benefit to alleviate thermal effect. The left side of laser crystal is coated with high transmission (HT) at 808 nm and high reflection (HR) at 1064 nm to act as an input mirror of the laser cavity. The right-hand side of the laser crystal is coated with antireflection (AR) at 808 nm and 1064 nm to reduce the intra-cavity loss. The output coupler is a plane-parallel mirror, whose reflectivity is 90% at 1064 nm and the cavity length is approximately 25 mm. The longitudinal-mode spacing $\Delta\nu_L$ is about 6 GHz, the relation between the longitudinal-mode spacing and the transverse-mode spacing is written as [28]:

$$\Delta\nu_T = \Delta\nu_L\left[\frac{1}{\pi}\cos^{-1}\left(\sqrt{1-\frac{L}{R}}\right)\right] \quad (3)$$

Where $\Delta\nu_L$=6 GHz, L=20 mm and R is the reflectivity of the output coupler, the transverse-mode spacing $\Delta\nu_T$ is found to be 0 GHz for a plane-parallel mirror, respectively. The small $\Delta\nu_T$ is conducive to keep the stability of transverse patterns and assist nonlinear coupling. The output power is received by power meter (Thorlabs PM100D), the output laser beam profiles are recorded by a beam profile analyzer (Spiricon PYROCAM IIIHR) and a charge-coupled device (CCD) camera. In addition, a part of the beam is interfered with the plane wave reference beam in a Mach–Zehnder interferometer to confirm the phase helicity of OVAs obtained in our experiment.

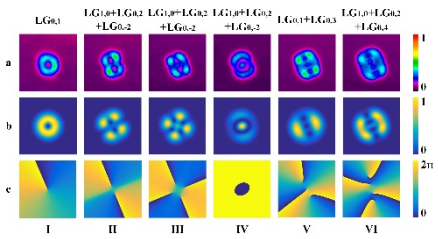

Fig. 2. Beam patterns formation from spontaneous TML of LG modes observed in the Nd:YVO_4 laser: (a) representative experimental results (I: 2.42 W; II: 3.25 W; III: 4.24 W; IV: 4.56 W; V: 5.10 W; VI: 5.82 W), (b) the simulated beam intensities, the corresponding simulated LG modes are listed at the top, (c) the corresponding phases.

When the optical axis of the axicon is coincident with the y-axis light (Δx=0.0 mm), six different beam profiles within the incident pump power (P_{in}) range from 2.20 W to 6.47 W are shown in Fig. 2(a). A stable doughnut-shaped $LG_{0,1}$ mode (P_{in}=2.42 W) is obtained when P_{in} reaches 2.4 W. The beam profile switched from $LG_{0,1}$ mode to the two-vortex mode (P_{in}=3.25 W) when P_{in} exceeds 3.2 W. As increasing P_{in} over 4.2 W, the four-vortex array beam (P_{in}=4.24 W) and the $LG_{1,0}$ mode-like radial symmetric beam profile (P_{in}=4.56 W) appears. When P_{in} is further increased higher than 5 W, the complex three-vortex array (P_{in}=5.10 W) and four-vortex array (P_{in}=5.82 W) in radial direction are observed. The four-vortex array in radial direction still remains stable when P_{in} is increased to 6.5 W. Considering the thermal effect and damage threshold of laser material, P_{in} is not further increased. The beam pattern orientation becomes slightly offset from the z-axis probably due to the imperfectly symmetrical distribution of the gain on the laser crystal.

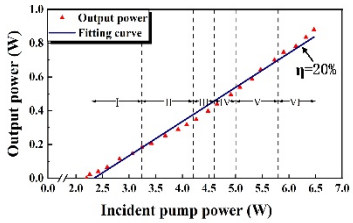

Fig. 3. OVAs formation from TML of LG modes and output power of the CW Nd:YVO_4 laser versus the incident pump power. I: $LG_{0,1}$ mode, II: two-vortex array, III: four-vortex array, IV: $LG_{1,0}$ mode, V: three-vortex array in radial direction, and VI: four-vortex array in radial direction.

The threshold pump power for aforementioned six different OVAs (I: $LG_{0,1}$ mode, II: two-vortex array, III: four-vortex array, IV: $LG_{1,0}$ mode, V: three-vortex array in radial direction, and VI: four-vortex array in radial direction.) are 2.20 W, 3.20 W, 4.20 W, 4.55 W, 5.00 W, and 5.80 W, respectively, as shown in Fig. 3. Each OVA is stable within a certain range. The output power increases linearly with P_{in} and the slope efficiency is approximately 20%. The maximum output power is 0.88 W at P_{in} is 6.47 W and the optical conversion efficiency is calculated to be 13.6%. A higher output power and more complicated OVA can be obtained with further increasing P_{in}.

The theoretically simulated beam profiles provided by Matlab look similar to the experimental beam profiles, as shown in Fig. 2(b). The first column is a $LG_{0,1}$ mode, and OVAs formation from TML of LG modes in a frequency-degenerated family ($2p+|l|=2$) are established by numerical simulation in the second, third and fourth column. Three different beam patterns under the circumstances are due to the competitive coefficients of three LG modes of such frequency-degenerated family. The weights $g_{1,0}$, $g_{0,2}$, and $g_{0,-2}$ for generating a stable two-vortex array in the second column are 0.55, 1.35 and 0.45, respectively. Further increasing P_{in}, the increasing input power leads to increasing of both $g_{1,0}$ and $g_{0,-2}$, in particular, $g_{0,-2}$ reaches the same level as $g_{0,2}$, as a result, a four-vortex array is formed ($g_{1,0}=0.95, g_{0,2}=0.85, g_{0,-2}=0.85$) in the third column. And in the fourth column, $g_{1,0}$ plays a major role, $g_{0,2}$ and $g_{0,-2}$ almost go down to zero ($g_{1,0}$=0.52, $g_{0,2}$=0.08, $g_{0,-2}$=0.08) when P_{in} continuously increases. It is a typical behavior for TML of a single frequency-degenerated family of LG modes [16,17]. Meanwhile, for the beam profiles in last two columns, TML of LG modes in different frequency-degenerate families occurs. The three-vortex array in radial direction is a result of TML of $LG_{0,1}$ mode ($2p+|l|=1$) and $LG_{0,3}$ mode ($2p+|l|=3$) ($g_{0,1}$=0.57, $g_{0,3}$=0.92). And the four-vortex array in radial direction is due to TML of $LG_{1,0}$, $LG_{0,2}$ modes ($2p+|l|=2$) and $LG_{0,4}$ mode ($2p+|l|=4$) ($g_{1,0}$=0.53, $g_{0,2}$=0.8, $g_{0,4}$=1.08). And it shows that the transition from optical vortex arrays formed in a single frequency-degenerate family of Laguerre-Gaussian modes to optical vortex arrays formed in different frequency-degenerate families of Laguerre-Gaussian modes has been achieved spontaneously. Although different frequency-degenerated families in a cavity usually have different optical frequencies, the frequency interval of transverse modes for a Fabry-Perot cavity might be small enough to achieve TML of different frequency-degenerated families [24]. The phases of the simulated profiles are expressed in Fig. 2(c), the corresponding phase singularities from the first column to the last column are 1, 2, 4, 0, 3 and 4, respectively.

The phase helicity of OVAs obtained in our experiment is verified by the Mach–Zehnder interferential method, as shown in Fig. 4(a1) and (a2). The measured interference fringes of the $LG_{0,1}$ mode and two-vortex array show that the corresponding phase singularities are 1 and 2, and the topological charge l of the $LG_{0,1}$ mode and two-vortex array are both 1, which has a good agreement with the simulated interference patterns in Fig. 4(b1) and (b2). The phase helicity of two-vortex array fits the features of two-vortex array formed in TML of a single frequency-degenerated family of LG modes in Fig. 2(c).

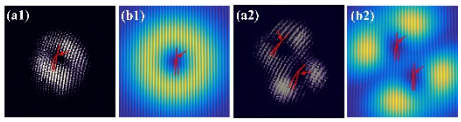

Fig. 4. (a1) (a2) fork interference pattern of the doughnut mode and the two-vortex array, (b1) (b2) the interference pattern of the simulated doughnut mode and two-vortex array and the red arrows point to the forked fringes.

TML of LG modes in different frequency-degenerate families can be actively controlled by the position of axicon, as shown in Fig. 5(a). The position of the axicon is defined as the Origin (0,0), which dominates the centrosymmetric center of annular beam in Fig. 1(a), and when the axicon moves along the negative direction of the x-axis, the pump beam profile is transformed to a decentered annular beam, as shown in Fig. 1(a) - (c), that is, the outer ring stays almost unchanged, the inner ring moves along the positive direction of the x-axis. The $LG_{0,1}$ mode is obtained When the decentered distance Δx stay at 0. The two-vortex array is achieved (P_{in}=3 W) within Δx<100 μm and the separation between two holes is increased with the enlarging Δx in Fig. 5(a2) - (a4). However, two-vortex array is replaced by a flat-topped beam at Δx>100 μm, which is attributed to the pump beam profile matched better with the Gaussian mode rather than the LG mode when Δx is too large [22].

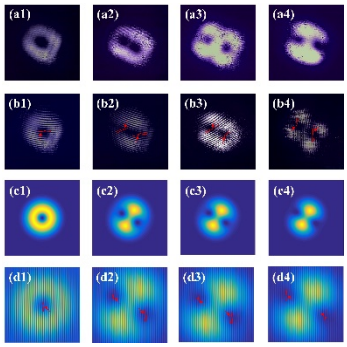

Fig. 5. (a1) - (a4) beam patterns with the axicon at different positions along the positive direction of the x-axis, (b1) - (b4) the fork interference patterns obtained in our experiment and the red arrows point to the forked fringes, (c1) - (c4) the simulated beam intensities, (d1) - (d4) the fork interference patterns of the simulated beam.

The fork interference patterns of the evolution from $LG_{0,1}$ mode to the two vortex array are measured in Fig. 5(b). The topological charge l is 1 in Fig. 5(b1) and two forklike fringes with opposite directions are obtained in Fig. 5(b2) - (b4), which are different from the case in Fig. 4(a2). It shows that the corresponding phase singularity is 2 and the topological charge l is 1 and -1, respectively. These results in Fig. 5(a) are similar to those in Ref.

[22] and we think that TML of LG modes in a frequency-degenerated family (*2p+|l|=2*) in Fig. 4(a2) is broken by a decentered annular pump beam. It actually is a result of TML of $LG_{0,0}$ mode (*2p+|l|=0*), $LG_{0,1}$ mode, $LG_{0,-1}$ mode (*2p+|l|=1*) and $LG_{1,0}$ mode (*2p+|l|=2*), which is shown as numerical simulations in Fig. 5(c). There is a $LG_{0,1}$ mode in Fig. 5(c1) and two vortex array in Fig. 5(c2), which is a result of TML of $LG_{0,1}$ mode, $LG_{0,-1}$ mode (*2p+|l|=1*) and $LG_{1,0}$ mode (*2p+|l|=2*) [22]. As Δx growing, the decentered annular pump beam makes the $LG_{0,0}$ mode oscillate, a $LG_{0,0}$ mode is introduced into TML of LG modes and the separation between two holes is dependent on the weight of the coefficient of $LG_{0,0}$ mode. Simulated Beam patterns with the continuous variation of separation between two holes in Fig. 5(c3) - (c4) are due to the different weights of the coefficient of $LG_{0,0}$ mode ($g_{0,0}$=0.04, $g_{0,1}$=0.32, $g_{0,-1}$=0.32, $g_{1,0}$=0.35) and ($g_{0,0}$=0.12, $g_{0,1}$=0.32, $g_{0,-1}$=0.32, $g_{1,0}$=0.25), respectively. Two vortex arrays can be replaced by the flat-topped beam when the weight $g_{0,0}$ continuously increases. The simulated fork interference patterns in Fig. 5(d) matches well with the experimental results obtained in our experiment. It proves once again that decentered annular beam pumping is an effective way to achieve OVAs generation of LG modes in different frequency-degenerate families.

In summary, we have experimentally obtained spontaneous TML of LG modes in different frequency-degenerate families based on an end-pumped Nd:YVO_4 laser pumped by an annular beam. The maximum output power of OVAs is 0.88 W and the optical conversion efficiency is 13.6%. OVAs generation of LG modes in different frequency-degenerate families can be actively controlled by adjusting the position of the axicon. This work paves a road to produce OVAs formation from TML of different frequency-degenerate families based on an annular beam. Quasi-Watt-level OVAs provide a potential stage for a variety of special applications, such as 3D displays.

Funding. National Natural Science Foundation of China (Project nos.61411130312 and 61308053); Guangdong Provincial Key Laboratory of Semiconductor Micro Display (2020B121202003); Foshan Science and Technology Bureau.

Disclosures. The authors declare no conflicts of interest.

Data Availability. Data underlying the results presented in this paper are not publicly available at this time but may be obtained from the authors upon reasonable request.

References

1. L. Allen, M.W. Beijersbergen, R.J.C. Spreeuw, and J.P. Woerdman. "Orbital angular momentum of light and the transformation of Laguerre-Gaussian laser modes," Phys. Rev. A. 45, 8185-8189 (1992).
2. C. Lobo and Y. Castin. "Nonclassical scissors mode of a vortex lattice in a Bose-Einstein condensate," Phys Rev. A. 72, 043606 (2005).
3. M. Padgett, R. Bowman. "Tweezers with a twist," Nat. Photon. 5, 343–348 (2011).
4. A.E. Willner, H. Huang, Y. Yan, Y. Ren, N. Ahmed, G. Xie, C. Bao, L. Li, Y. Cao and Z. Zhao. "Optical communications using orbital angualr momentum beams," Adv. Opt. Photonics. 7, 66-106 (2015).
5. X.F. Li, J.Q Chu, Q. Smithwick and D.P. Chu. "Automultiscopic displays based on orbital angular momentum of light," J. Opt. 18, 085608 (2016).
6. A.Y.G. Fuh, Y.L. Tsai, C.H. Yang and S.T. Wu. "Fabrication of optical vortex lattices based on holographic polymer-dispersed liquid crystal films," Opt. Lett. 43, 154–157 (2018).
7. E. Calisto, M.G. Clerc, M. Kowalczyk and P. Smyrnelis. "On the origin of the optical vortex lattices in a nematic liquid crystal light valve," Opt. Lett. 44, 2947-2950 (2019).
8. V.Y. Bazhenov, M.S. Soskin and M.V. Vasnetsov. "Screw dislocations in light wave-fronts," J. Mod. Opt. 39, 985–990 (1992).
9. J.A. Anguita, J. Herreros and I.B. Djordjevic. "Coherent multimode OAM superpositions for multidimensional modulation," IEEE Photon. J. 6, 7900811 (2014).
10. Y.F. Chen and Y.P. Lan. "Formation of optical vortex lattices in solidstate microchip lasers: Spontaneous transverse mode locking," Phys. Rev. A. 64, 063807 (2001).
11. Y. Shen, Z. Wan, X. Fu, Q. Liu and M. Gong. "Vortex lattices with transverse-mode-locking states switching in a large-aperture off-axis-pumped solid-state laser," J. Opt. Soc. Amer. B. 35, 2940-2944 (2018).
12. K. Otsuka and S.C. Chu. "Generation of vortex array beams from a thin-slice solid-state laser with shaped wide-aperture laser-diode pumping," Opt. Lett. 34, 10–12 (2019).
13. D. Naidoo, K. Aït-Ameur, M. Brunel and A. Forbes. "Intracavity generation of superpositions of Laguerre–Gaussian beams," Appl. Phys. B. 106, 683-690 (2012).
14. J. Dong, X. Wang, M. Zhang, X. Wang and H. He. "Structured optical vortices with broadband comb-like optical spectra in Yb:Y3Al5O12/YVO4 Raman microchip laser," Appl. Phys. Lett. 112, 161108 (2018).
15. G. Lin, Y. Cao, Z. Lu and Y.K. Chembo. "Spontaneous generation of orbital angular momentum crystals using a monolithic Nd:YAG nonplanar ring laser," Opt. Lett. 44, 203 (2019).
16. M. Brambilla, F. Battipede, L.A. Lugiato, V. Penna, F. Prati, C. Tamm and C.O. Weiss. "Transverse laser patterns. I. Phase singularity crystals," Phys. Rev. A. 43, 5090-5113 (1991).
17. J. Scheuer and M. Orenstein. "Optical vortices crystals: Spontaneous generation in nonlinear semiconductor microcavities," Science, 285, 230 (1999).
18. D.H. Auston. "Transverse mode locking," IEEE J. Quantum Electron. 4, 420–422 (1968).
19. H. Yu, H. Zhang, Z. Wang, J. Wang, Z. Pan, S. Zhuang and D. Tang. "Experimental observation of optical vortex in self-frequency-doubling generation," Appl. Phys. Lett. 99, 41102 (2011).
20. Y. Toda, S. Honda and R. Morita. "Dynamics of a paired optical vortex generated by second-harmonic generation," Opt. Express. 18, 17796–17804 (2010).
21. M. Zhang, H. He and J. Dong. "Decentered Gaussian beam pumped highly efficient passively Q-switched microchip laser for controllable high-order transverse modes," IEEE Photonics J. 9, 1501214 (2017).
22. Y. Pan, M. Zhang and J. Dong. "Orientation and separation controllable dual vortex passively Q-switched microchip laser," J. Opt. 21, 085202 (2019).
23. Z. Zhang, K. Gui, C. Zhao, Y. Xing and H. Zhang. "Direct generation of vortex beam with a dual-polarization microchip laser," IEEE Photon. Tech. Lett. 31, 1221-1224 (2019).
24. Z. Zhang and C. Zhao. "Intra-cavity generation of linearly distributed and continuously varied optical vortices," IEEE Photon. Tech. Lett. 32, 196-199 (2020).
25. Z. Zhang and C. Zhao. "Spontaneous phase and frequency locking of transverse modes in different orders," Phys. Rev. Appl. 3, 024010 (2020).
26. D.J. Kim and J.W. Kim. "Direct generation of an optical vortex beam in a single-frequency Nd:YVO_4 laser," Opt. Lett. 40, 399-402 (2015).
27. M. Wei, Y. Lai and K. Chang. "Generation of a radially polarized laser beam in a single microchip Nd:YVO_4 laser," Opt. Lett. 38, 2443-2445 (2013).
28. Y.F. Chen and Y.P. Lan. "Transverse pattern formation of optical vortices in a microchip laser with a large Fresnel number," Phys. Rev. A. 65, 013802 (2001).